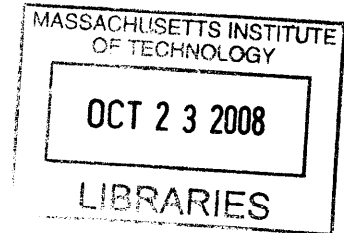


**Characterization and Modeling of  
Pattern Dependencies and Time Evolution  
in Plasma Etching**

By  
Ali Farahanchi



Submitted to the Department of Electrical Engineering and Computer Science  
in Partial Fulfillment of the Requirements for the Degree of  
Master of Engineering in Electrical Engineering and Computer Science

at the Massachusetts Institute of Technology  
*[June 2008]*  
May, 2008

©2008 Massachusetts Institute of Technology  
All rights reserved.

Author \_\_\_\_\_

*[Signature]*  
Electrical Engineering and Computer Science  
May 23, 2008

Certified by \_\_\_\_\_

*[Signature]*  
Duane S. Boning  
Professor of Electrical Engineering and Computer Science  
Thesis Supervisor

Accepted by \_\_\_\_\_

*[Signature]*  
Arthur C. Smith  
Chairman, Department Committee on Graduate Theses  
Electrical Engineering and Computer Science

**ARCHIVES**



# **Characterization and Modeling of Pattern Dependencies and Time Evolution in Plasma Etching**

By

Ali Farahanchi

Submitted to the  
Department of Electrical Engineering and Computer Science

May 23, 2008

In Partial Fulfillment of the Requirements for the Degree of  
Master of Engineering in Electrical Engineering and Computer Science

## **ABSTRACT**

A quantitative model capturing pattern dependent effects and time evolution of the etch rate in Deep Reactive Ion Etching (DRIE) is presented. DRIE is a key process for pattern formation in semiconductor fabrication. Non-uniformities are caused due to microloading and aspect ratio dependencies. The etch rate varies over time and lateral etch consumes some of the etching species. This thesis contributes a physical analysis for capturing and modeling microloading, aspect ratio dependencies, effects of lateral etch and time evolution of the etch rate. This methodology is applied to the study of etching variation on silicon wafers; the integrated model is able to predict pattern density and feature size dependent non-uniformities in trench depth and time evolution of the etch rate. Previous studies of variation in plasma etching have characterized microloading and aspect ratio dependent etching (ARDE) as distinct constant causes for etch non-uniformity. In contrast to these previous works, we present here a time-based methodology for vertical and lateral etch.

Thesis Supervisor: Duane S. Boning

Title: Professor of Electrical Engineering and Computer Science

## **Acknowledgements**

I would like to thank my advisor, Professor Duane Boning, for the opportunity to work with him and for his continuous support throughout my research as a UROP student and later as an MEng student in his group. Without his guidance, I would not have reached this milestone. I would like to continue by thanking the current and past members of the Statistical Metrology Group who have been there for me by giving me the inspirations that have allowed me to progress. Kwaku O. Abrokwah, Ajay Somani, Edward Paul, Karen González-Valentín Gettings, Xiaolin Xie, Hong Cai, Nigel Drego, Karthik Balakrishnan, Daihyun Lim, Daniel Truque, Albert Chang, Wei Fan, Joy Johnson, and Zhipeng Li, thank you for your friendship.

I would like to thank my family for the love, guidance, and support they have provided me with throughout my life. I certainly could not have made it this far without them.

I would also like to especially thank my friend and my mentor Hayden Taylor, who has guided and tutored me throughout my research. Thank you for your encouragement and countless insights and hints about my work.



# Table of Contents

- ABSTRACT.....3
- Acknowledgements.....4
- Chapter 1 Introduction and Motivation.....6
- Chapter 2 A Semi-Empirical Model for Etching Non-uniformities .....8
  - 2.1 Micro-loading .....8
  - 2.2 ARDE.....10
  - 2.3 Integrated model for etch rate .....11
- Chapter 3 Improved Model for Etch Rate: Vertical and Lateral .....12
  - 3.1 Etchants flux .....12
  - 3.2 Improved integrated model for etch rate.....15
  - 3.3 Lateral etch rate.....16
- Chapter 4 Mask Description .....19
  - 4.1 Nominal pattern density.....21
  - 4.2 Effective pattern density .....22
- Chapter 5 Experiment in Non-uniformity and Time Evolution of DRIE .....24
  - 5.1 Optical interferometer .....25
  - 5.2 Scanning electron microscope .....28
- Chapter 6 Etch Rate Model: Data and Fitting.....32
  - 6.1 Pattern Dependency of Etch Rate .....32
  - 6.2 Time Evolution of Etch Rate .....34
  - 6.3 Lateral Etch Rate.....37
- Chapter 7 Integrated Model for Time Dependent Etching .....39
- Chapter 8 Conclusion and Future Work .....40
- Appendix A.....41
- References.....43

# Chapter 1

## Introduction and Motivation for Research

Deep Reactive Ion Etch (DRIE) is one of the current technologies in semiconductor fabrication. This thesis focuses on studying variations and time evolution of DRIE. Previous work has shown a strong relationship between etching non-uniformities and pattern density [1]. Intuitively, the etch rate is lower in the regions on the silicon wafer that have more open areas that will be exposed to etching. This is simply due to the fact that there is more competition for reactant species in the regions with large open areas. If the percentage of open area is described as the pattern density, it is concluded that etch rate is a decreasing function of pattern density. This relation is also called the micro-loading effect.

Besides micro-loading there is also another effect referred to as macro-loading. According to Sun et al. [2] the global etch rate map is dependent on the overall pattern density of the wafer. Macro-loading and its effect on non-uniformity is described in the next chapter; however, it is not the main focus of this thesis.

Macro-loading and micro-loading describe the dependency of the etch rate on the pattern density. However, it has been shown [1] that the dominant cause of etching non-uniformities at the feature scale is the variation of etch rate based on the aspect ratio (Aspect Ratio Dependent Etch, or ARDE for short). This effect which essentially is a feature-level phenomenon, is based on the transport of the etchant reactant through the micro-structure features on the silicon wafer.

Previous studies [1] have proposed a semi-empirical model to predict the effects of micro-loading and ARDE on the etch rate. In that model the etch rate is assumed to be a constant over the etch time, hence the etch depth is a linear function of time.

On the other hand, as will be shown in this thesis, ARDE is not limited to vertical etch but rather is also an important factor that determines the lateral etch rate. Since the overall consumption of the reactant species is divided between the vertical etch and the lateral etch, the vertical etch rate is lower than what it is predicted in the previous semi-empirical model (which only considers the vertical etch).

Chapter 2 will describe the semi-empirical model in more detail. In Chapter 3, I will introduce the improvements to the semi-empirical model. These improvements are the foundation for the experiment and metrology of this thesis. Chapter 4 will describe the mask design that is used for the DRIE experiment. In Chapter 5, the DRIE experiment itself will be explained. The last two chapters will explain the characterization and modeling of the etch rate (vertical and lateral) based on the improved model and the measurements from the DRIE experiment. Finally, conclusions and suggestions for future work will be presented in Chapter 10.

## Chapter 2

### A Semi-Empirical Model for Etching Non-uniformities

This chapter explains the semi-empirical model that K. Abrokwah [1] introduced in his work, including the physical intuition behind this model. The two main causes of the etching non-uniformities are identified as pattern density (micro-loading) and aspect ratio dependency (ARDE). Each of these effects are physically modeled and described with an equation and the overall etch rate is described in a multiplicative integrated model. We first consider pattern dependencies involving pattern density and micro-loading.

#### 2.1 Micro-loading

As stated earlier, the micro-loading effect describes the fact that the etch rate is a decreasing function of pattern density. This is because there is a higher competition for the etchant reactants in the areas of the wafer that are higher in pattern density (i.e. having more open area). It is important to notice that the micro-loading effect at each point on the wafer is not only a function of the pattern density of that specific point but also is a function of the pattern density of the neighboring areas. In other words, the competition for etchant reactants is localized within a radius. This radius, also known as the characteristic distance for effective pattern density, determines in how big of an area the competition for etchant reactants is localized.

Effective pattern density is calculated by convolving the actual or local layout pattern density with an averaging filter. The width of the filter is representative of the distance over which the average of the pattern density is calculated. The larger the width of the filter is, the smoother the effective pattern density is. An example of calculating effective pattern density is shown in Figure 2.1.

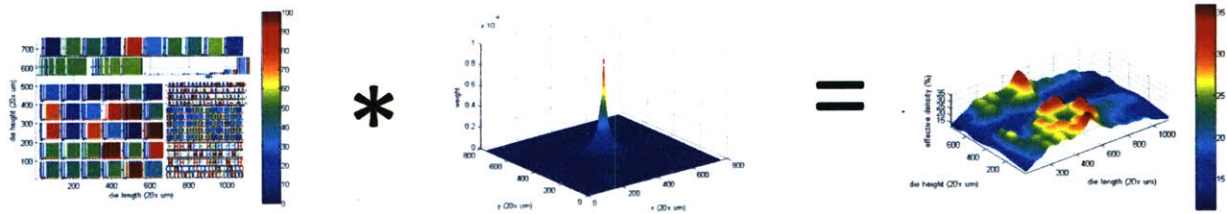


**Figure 2.1 – The 3-D map for effective pattern density is calculated by convolving the layout pattern density and the averaging filter [1].**

In Figure 2.1, the left colored graph shows the actual or local pattern density for a die. The graph in the middle represents the averaging filter that is used for calculating the effective pattern density. In this figure, the filter has the following form:

$$f(r) = \frac{a}{(r + c)^2} \tag{2-1}$$

The filter function is azimuthally symmetric. The constant  $c$  is the characteristic distance of the filter and its value will be fit to match the data from the experiment. The constant  $a$  is used to keep the function  $f(r)$  normalized. It is worthwhile to notice that other forms of filter function can be used as long as it is decreasing with distance (Figure 2.2). It can be shown that only the characteristic distance plays a critical role in the effective pattern density model for etching and not the actual function of the filter itself [1].

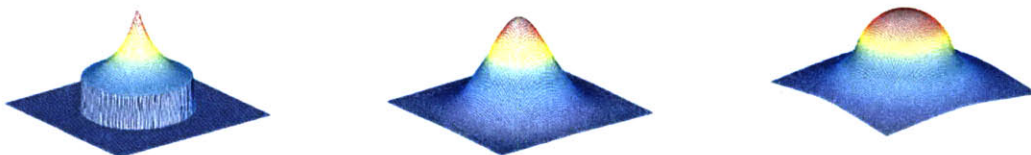


**Figure 2.2 – The 3-D profiles for various averaging filters [1].**

## 2.2 ARDE

As mentioned before, ARDE is based on the transport of the reactant species through the micro-structure features. The reactants that enter a feature and transport all the way to the bottom will have the chance for etching the wafer if they get attached to the silicon. In the model developed by K. Abrokwah [1], this situation is described using the Knudson transport model. According to the Knudson model, the ratio between the fluxes of the reactants at the top and at the bottom of the feature can be calculated by knowing two physical parameters;  $k$ , which is known as the Knudson coefficient and equals the probability of transporting from the top to the bottom, and  $s$ , which is the probability that a reactant at the bottom will actually etch the feature. Figure 2.3 shows this model.

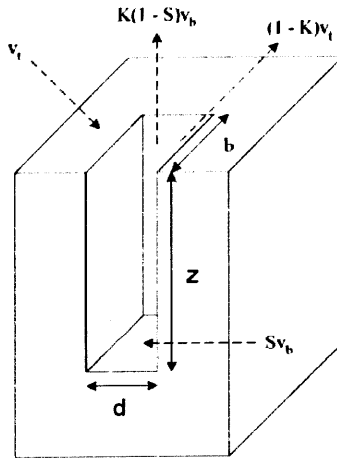


**Figure 2.3 – Schematic of etchant flux in narrow trench feature [1].**

Equation 2-2 shows the relationship between the etch rates at the top and the bottom:

$$\frac{R_{bottom}}{R_{top}} = \frac{flux_{bottom}}{flux_{top}} \frac{k}{k + (1-k)s} \quad (2-2)$$

where  $flux_{bottom}$  and  $flux_{top}$  denote the flux of etching species through the bottom and top surface areas (in units of  $cm^{-2}s^{-1}$ ), respectively.

### 2.3 Integrated model for etch rate

Equations 2-1 and 2-2 describe the two main factors that cause the etching non-uniformities, pattern density and feature size. The integrated model for etch rate combines these two equations in the following form:

$$z(x, y, t) = t \left( R_0 e^{-\alpha \rho_{eff}(x, y)^\beta} \right) \left( \frac{k}{k + (1 - k)s} \right) \quad (2-3)$$

where  $t$  is the etching time,  $R_0$  is the effective blanket etching rate, and  $\rho_{eff}(x, y)$  is the effective pattern density as a function of position on the die.

Two assumptions are important in writing Equation 2-3. First, the effective pattern density shows itself in an exponential form with two fitting parameters,  $\alpha$  and  $\beta$ . The fitting parameters are optimized by matching Equation 2-3 with experimental data. Secondly, we see that Equation 2-3 describes the etch depth,  $z$ , as a linear function in time. This is based on the assumption that the etch rate remains constant over the course of etching. As will be described in the next chapter, this assumption can be improved.

Two improvements to Equation 2-3 will be introduced in the next chapter. The first change will be made by considering a more accurate Knudsen transport model that takes into account the lateral etch as well as the vertical etch. A new parameter, sticking factor to the side wall, will be introduced to characterize the lateral etch. The second change will consider that the etch rate is not constant over time and therefore the etch depth is not a linear function of time.

## Chapter 3

### Improved Model for Etch Rate: Vertical and Lateral

The first part of this chapter will develop a model that formulates the etch rate when both vertical and lateral etch are present. In the second part of the chapter, the lateral etch rate will be formulated. These derivations follow the approach by Abrokwah et al. in [1], with extensions to handle the sidewall.

#### 3.1 Etchants flux

Figure 3.1 shows a schematic of an idealized cylindrical feature and the transport of the reactant species. Circles 1 and 2 are two imaginary rings around the perimeter of the feature with separation distance  $z$ . Each ring also defines a corresponding surface through which reactant species may pass.

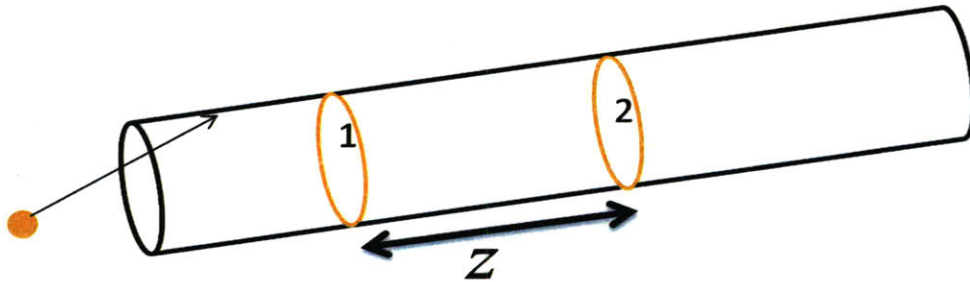


Figure 3.1 – Schematic of an idealized cylindrical feature.

To formulate the conductance of reactant species through the feature, four probabilities are introduced:



$p_{rr}(z)$  = Probability that a particle leaves ring 1 and directly strikes ring 2

$p_{rs}(z)$  = Probability that a particle leaves ring 1 and directly passes surface 2

$p_{sr}(z)$  = Probability that a particle leaves surface 1 and directly strikes ring 2

$p_{ss}(z)$  = Probability that a particle leaves surface 1 and directly passes surface 2

When a particle (etchant) strikes a ring, it collides with the side wall and may etch the sidewall with probability  $s$ , or may bounce off the sidewall with probability  $1-s$ . The next step is to write down the relationships between these probabilities. Since the ring is the differential of each surface, two additional equations can be written as:

$$p_{rr}(z) = -\frac{dp_{rs}}{dz} \quad (3-1)$$

$$p_{sr}(z) = -\frac{dp_{ss}}{dz} \quad (3-2)$$

Now let's assume just for a minute that the side wall etch is negligible, meaning that there is no sticking to the side wall and all the reactants that hit the side wall will bounce off the wall. In that case, according to the second law of thermodynamics, the sidewall must be in thermal equilibrium with the plasma gas. This means that there are as many reactants that go from a ring (side wall) to a cross section as there are reactants that go from the cross section to the ring. Therefore an equilibrium equation can be written as:

$$2\pi r \cdot p_{rs}(z)dz = \pi r^2 \cdot p_{sr}(z)dz \quad (3-3)$$

Or in a simpler form:

$$p_{rs}(z) = \frac{r}{2} \cdot p_{sr}(z) \quad (3-4)$$

However, in the more realistic case the side wall etching is small but not negligible. If  $s$  is the sticking factor to the sidewall, then only  $1-s$  fraction of the reactants that go from a cross section to a ring will come back from the ring to some cross section. Therefore Equation 3-3 can be modified into:

$$2\pi r \cdot p_{rs}(z)dz = (1-s) \cdot \pi r^2 \cdot p_{sr}(z)dz \quad (3-4)$$

Finally the equation that relates the Knudson coefficient  $k$  to the introduced probabilities is:

$$k = p_{ss}(L) + \int_0^L p_{sr}(z')q(z')dz' \quad (3-5)$$

where  $L$  is the depth of the feature, and

$$q(z) = p_{rs}(L-z) + \int_0^L p_{rr}(z'-z)q(z')dz' \quad (3-6)$$

The system consisting of Equations 3-1 to 3-6 needs to be solved to find the Knudson transport coefficient  $k$  in terms of the physical parameters of the model. A solution to these equations is suggested by Clausing [4]:

$$k(z) = \frac{1}{\gamma \left( \frac{z}{CD} \right) + \frac{1}{1-s_{side}}} \quad (3-7)$$

Here  $z$  is the feature depth,  $CD$  is the critical dimension (width) of the feature, and  $\gamma$  is a dimensionless factor that depends on the shape of the feature's cross section (for a circular cross section  $\gamma$  is 0.75). As emphasized in Equation 3-7, the Knudson coefficient is a function of  $z$  and therefore varies as the feature gets deeper during the etching process.

Equation 3-7 suggests that  $k$  decreases as the aspect ratio of the feature  $z/CD$  increases. This is expected to be true, since  $k$  represents the probability of transport for the reactants, and it is less likely for the reactants to go all the way through a feature with higher aspect ratio.

Equation 3-7 also suggests that  $k$  decreases as  $s$ , the sticking factor to the sidewall, increases. Again this result is expected to be true, since a stickier side wall decreases the chance of transport for the etchant reactants.

In the next step the newly calculated Knudson transport relationship is substituted for the old  $k$  in Equation 2-2:

$$R_{bottom}(t) = \frac{R_{top}}{\left(1 + \frac{s_{side} \cdot s_{bottom}}{1 - s_{side}}\right) + \gamma \left(\frac{z(t)}{CD}\right) s_{bottom}} \quad (3-8)$$

Equation 3-8 gives an etch rate as a function of time and feature depth. The assumption that the etch rate is constant over time is no longer required.

### 3.2 Improved integrated model for etch rate

Now that the new ARDE model is formulated, the two effects (ARDE and micro-loading) are incorporated in a multiplicative equation to complete the whole picture of the etch rate. Referring to Equation 2-3; we replace  $R_{top}$  with the pattern density dependence to get

$$R_{bottom}(x, y, t) = \frac{R_0 e^{-\alpha \rho_{eff}(x, y)^\beta}}{\left(1 + \frac{s_{side} \cdot s_{bottom}}{1 - s_{side}}\right) + \gamma \left(\frac{z(t)}{CD}\right) s_{bottom}} = \frac{\partial z}{\partial t} \quad (3-9)$$

Equation 3-9 represents the improved model for the etch rate. By integrating both sides, the relation between the etch depth and time is revealed:

$$t = \left( \gamma \frac{z^2}{2R_0 \cdot CD} s_{bottom} + \frac{z}{R_0} \left( 1 + \frac{s_{side} \cdot s_{bottom}}{1 - s_{side}} \right) \right) e^{\alpha \rho_{eff}(x,y)^\beta} \quad (3-10)$$

This equation will be used in the future chapters to explain the DRIE experimental data. There are a number of fitting parameters present in Equation 3-10, including  $\alpha$ ,  $\beta$ ,  $\gamma$ , sticking factors  $s_{side}$  and  $s_{bottom}$  for sidewall and bottom, and  $R_0$  (the effective blanket etch rate). The equation suggests that the etch depth is a quadratic function of time, meaning that the vertical etch rate eventually decreases as the feature gets etched deeper.

### 3.3 Lateral etch rate

Figure 3.2 shows a scanning electron microscope image of the profile of an etched feature. As expected for this non-isotropic etch chemistry, the sidewall is not even close to the vertical direction, and this simply shows that there is a comparably large lateral etch rate. To model the lateral etch rate one can notice that at the depth  $z$ , the sidewall is exposed to the etchant reactants for a time that depends on the depth:

$$t_{etch}(z) = T_{total} - t(z) \quad (3-11)$$

where  $T_{total}$  is the total etching time for the silicon wafer and  $t(z)$  is given by Equation 3-10.

Therefore the lateral etching distance at some depth  $z$  is:

$$x = R_{side-wall} \cdot t_{etch}(z) = R_{side-wall} (T_{total} - t(z)) \quad (3-12)$$

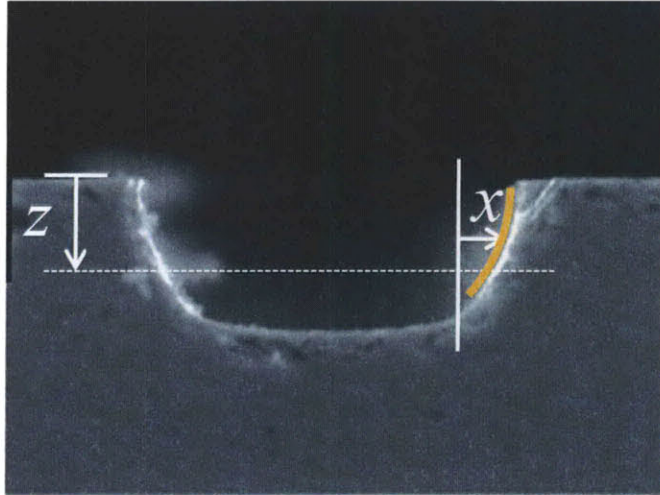


**Figure 3.2 – A scanning electron microscope image of the profile of an etched feature.  $x(z)$  describes the shape of the sidewall (also highlighted by the orange line). The image shows the existence of a significant lateral etch rate.**

If the feature has a low aspect ratio (the depth of the feature is much less than the width of the feature), the sidewall etch rate can be estimated if the etch rate at the top of the feature is known.

In this case

$$R_{side-wall} \approx \frac{S_{side}}{S_{bottom}} R_0 \quad (3-13)$$

and

$$x(z) \approx \frac{S_{side}}{S_{bottom}} R_0 (T_{total} - t(z)) \quad (3-14)$$

Thus, we see that the profile of the feature is the same function of depth as the time is. The orange line on Figure 3.2 shows that a quadratic function can be used to describe the profile of the feature, similar to that given by Equation 3-10.

Equations 3-10 and 3-14 are the final formulation for vertical and lateral etch in the DRIE experiment. In Chapter 6 these equations form the basis for matching to the experimental data of Chapter 5. There are six physical parameters that will be fit by applying Equations 3-10 and 3-14

to the experimental data, using an optimization procedure to minimize the sum of squared error between the model and experimental data. These parameters are  $\alpha$ ,  $\beta$ ,  $c$ ,  $s_{bottom}$ ,  $s_{side}$  and  $\gamma$ , where  $\alpha$  and  $\beta$  are pattern density rate parameters,  $c$  is the characteristic length of the averaging filter used for calculating the effective pattern density,  $s_{bottom}$  and  $s_{side}$  are the bottom and sidewall sticking coefficient, and  $\gamma$  is the geometric factor (Equation 3-7) that depends on the shape of the cross-section of the feature.

## Chapter 4

### Mask Description

The mask that is used for the DRIE experiment is 4 inches by 4 inches square, and originally is designed as a micro-fluidic MEMS test structure (courtesy of H. Taylor). It contains different structures including channels, squares, triangles, and reservoirs. The critical dimension of the features varies from one micron to one hundred microns. The mask design is shown in Figure 4.1.

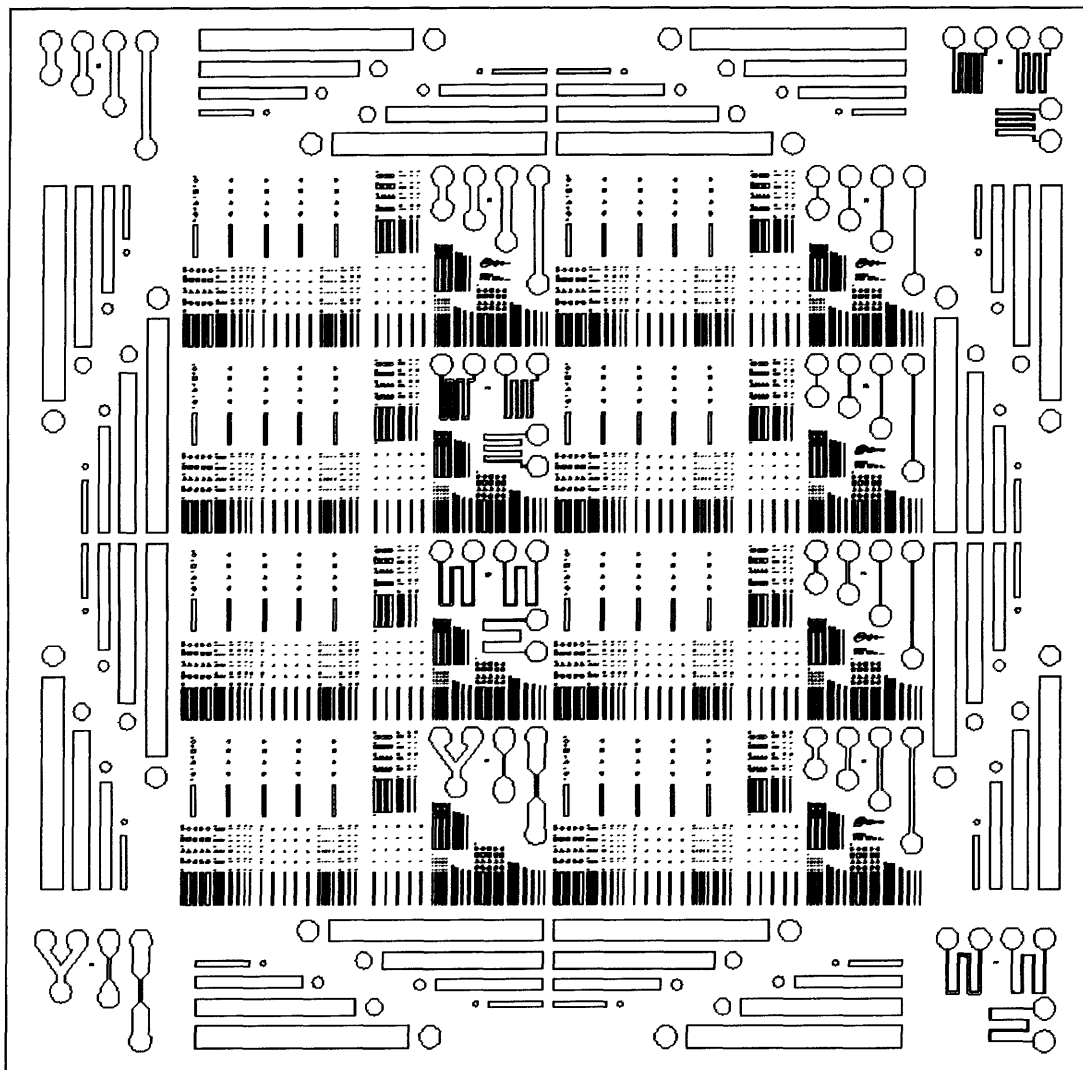
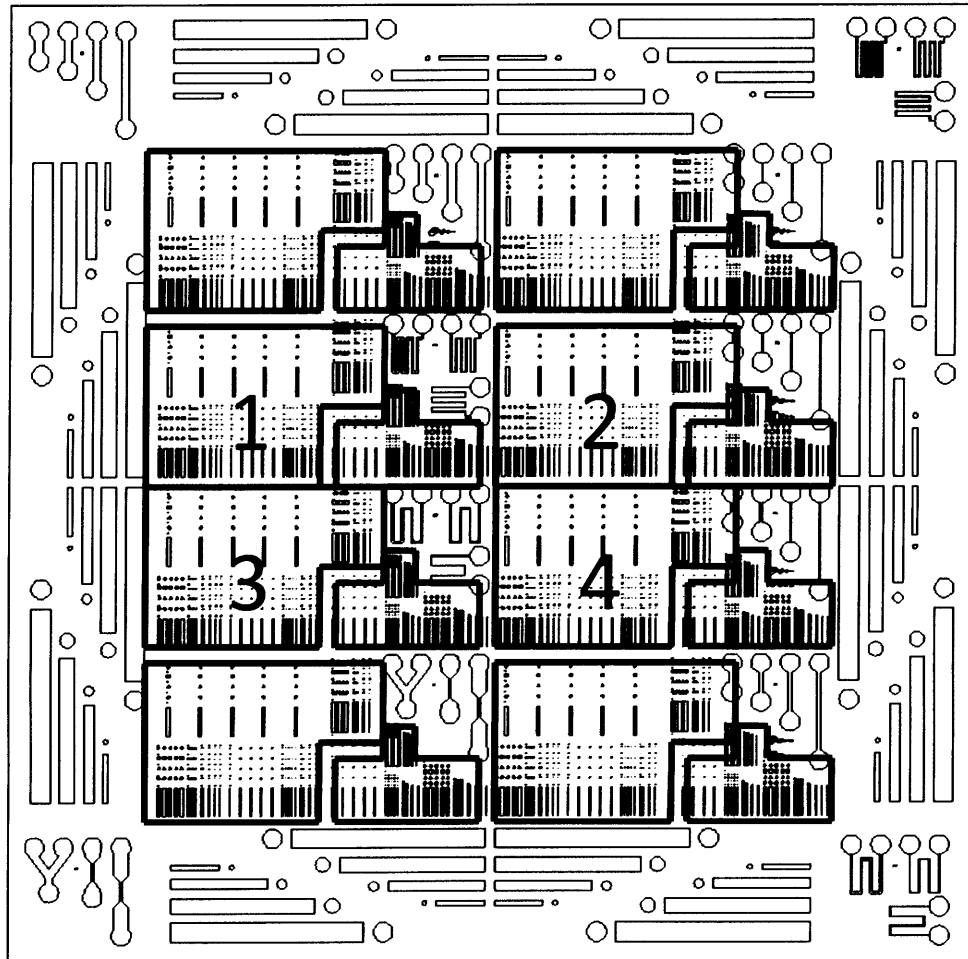


Figure 4.1 – Test mask layout.

There are eight dies on the wafer, four of which are used for taking the measurements (Figure 4.2). Measurements are taken from all of the channel structures on the four dies. Figure 4.3 shows an expanded view of one die where the blue arrows indicate the locations for measurements (optical interferometry and SEM). Chapter 5 describes the DRIE experiment and the measurement plans in more detail.



**Figure 4.2 – Die locations. The test mask includes eight dies and the measurements are taken from dies 1, 2, 3 and 4.**



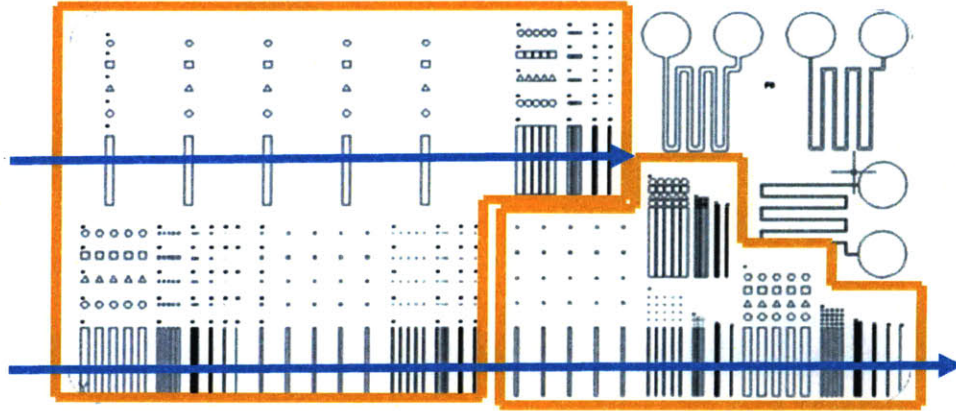


**Figure 4.3 – Close up view of a die. The measurements are taken from the channel structures, indicated by the blue arrows.**

#### *4.1 Nominal pattern density*

Based on the nominal values of the channel width (line width) and line space, the nominal layout pattern densities of the channel structures are calculated (Figure 4.4). The sixteen measurement locations at different line width and line space result in three different local pattern densities. Since the ratio of the line space and line width is either 0.1, one or 10, the nominal pattern density of the channels is 9%, 50%, or 91%. On the other hand, the effective pattern density of the channels is calculated by convolving the nominal pattern density map (above) with the spatial averaging filter. The next section shows an example of this calculation.

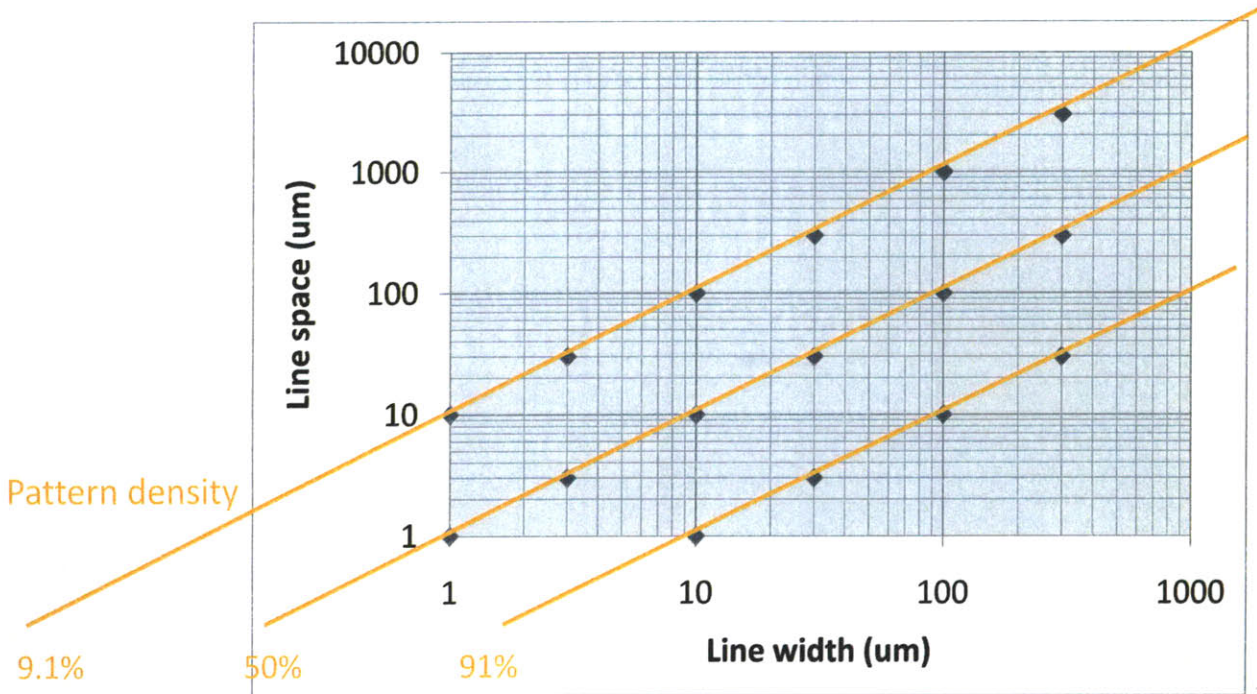


**Figure 4.4 – The design space of line width and line space and the corresponding nominal pattern densities.**

#### 4.2 Effective pattern density

The averaging filter that is used in this example has the form of Equation 2-1. The value of  $c$ , the characteristic length, is arbitrarily chosen in this example to be 200 microns. The actual value of the characteristic distance is later determined by fitting  $c$  to match the experimental data. Figure 4.5 shows the 3-D map of the effective pattern density, using this filter. We see the general “smoothing” of the local features into the averaged of regional effective pattern density.

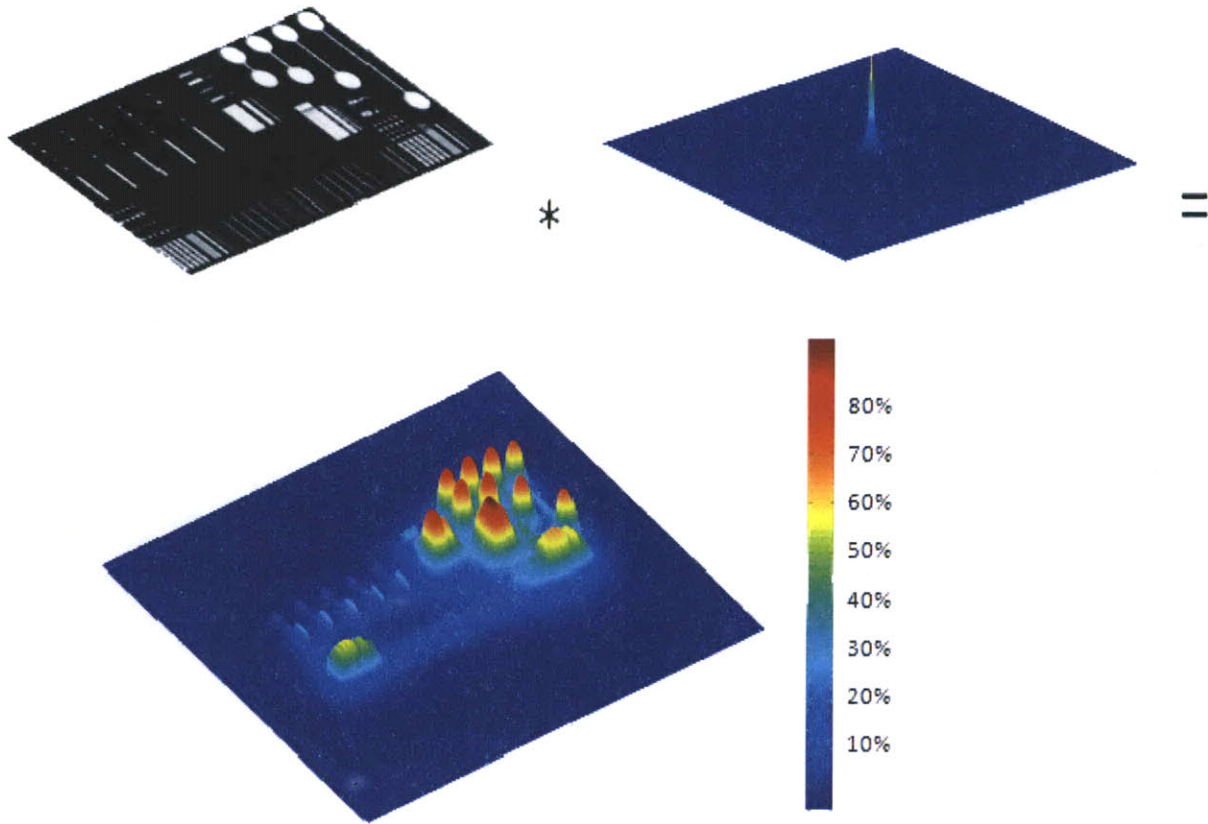


**Figure 4.5 – An example of calculating the effective pattern density, for our test mask.**

## Chapter 5

### Experiment in Non-uniformity and Time Evolution in DRIE

The improved model of etch rate developed in Chapter 3 explains the time evolution of the etch rate, as a function of both feature size and pattern density. To identify the accuracy of this model an extensive DRIE experiment is designed. Fifteen wafers are etched, each with a different exposure time. Table 5.1 shows the wafer numbers and the corresponding exposure time.

wafer #	etch time (sec)
1	40
2	80
3	120
4	160
5	200
6	240
7	280
8	320
9	360
10	400
11	440
12	480
13	520
14	560
15	600

➤ pattern density dependency

➤ lateral etch profile

➤ time evolution: vertical etch

**Table 5.1 – The total etch time for each wafer.**

The annotation to the right of the table shows which wafers are compared with which part of the etch rate model. All the wafers are etched using a similar recipe: continuous process (no time multiplexing) with SF6 and C4F8 under 60 mTorr pressures. Powers are set at 60 W (platen) and



800 W (Coil). Figure 5.1 shows a schematic of the plasma chamber and the actual picture of the STS Deep Reactive Ion Etching (DRIE) machine that is used for etching these fifteen wafers.

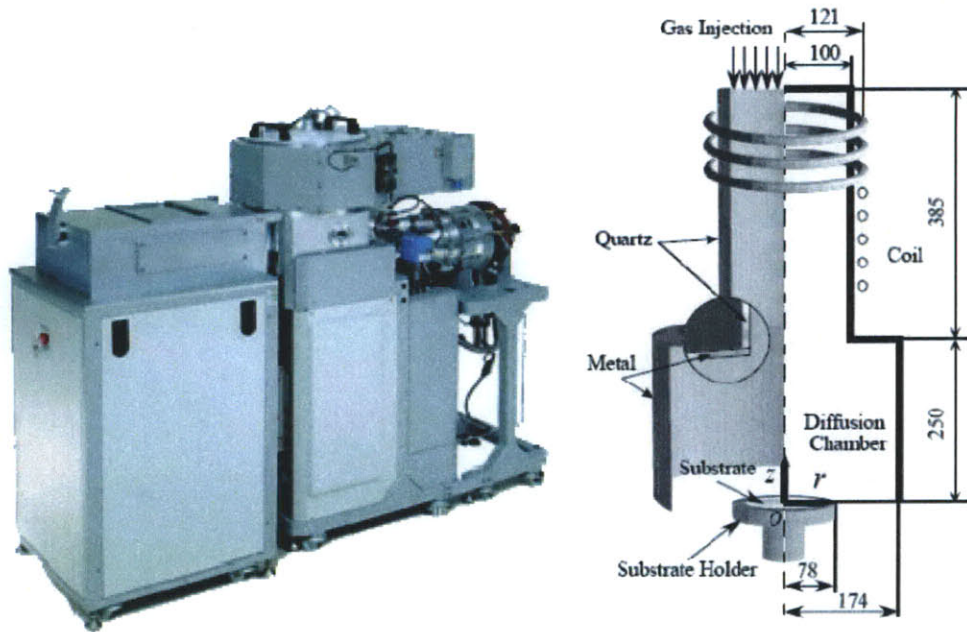


**Figure 5.1– The STS DRIE machine (left) and schematic of a plasma chamber (right) [1].**

### *5.1 Optical interferometer*

All the depth measurements are taken using a vertical scanning optical interferometer (Veeco, model Wyko-NT). The sample is translated vertically, such that each point on the surface passes through focus. Maximum fringe contrast of the white light source, which occurs at the point of best focus, is determined for each point on the surface. A few of the 3-D plots generated by the interferometer are shown in Figures 5.2 to 5.5.

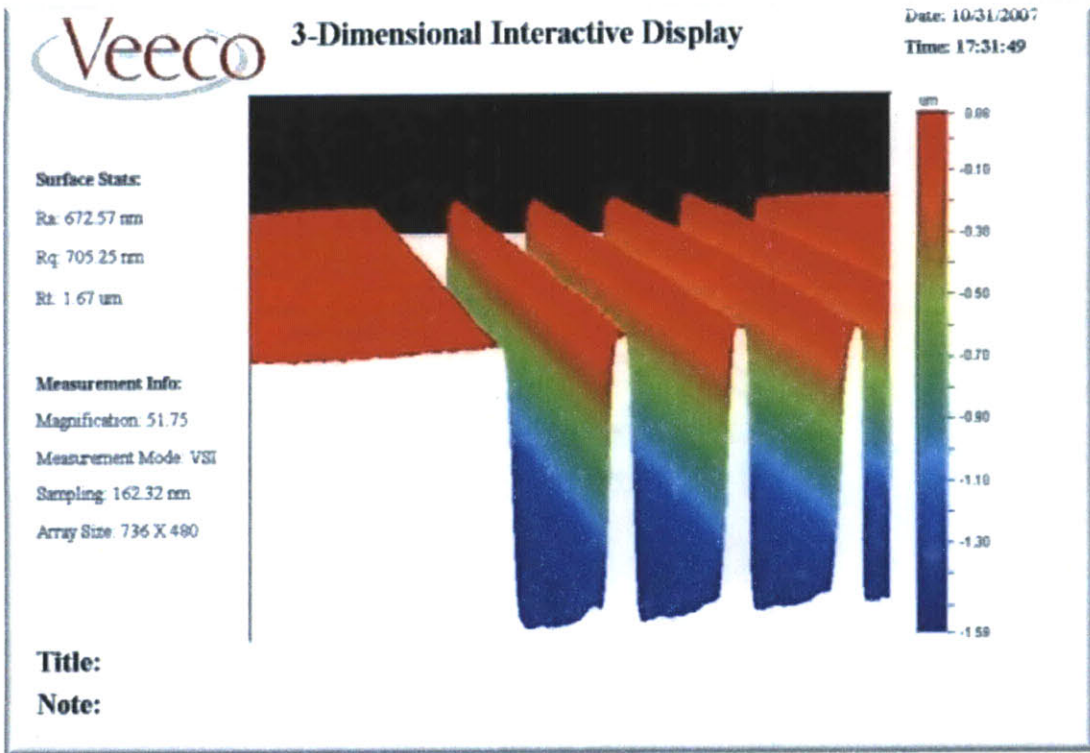


Figure 5.2 – 3-D image from optical interferometry of “channel” structures.

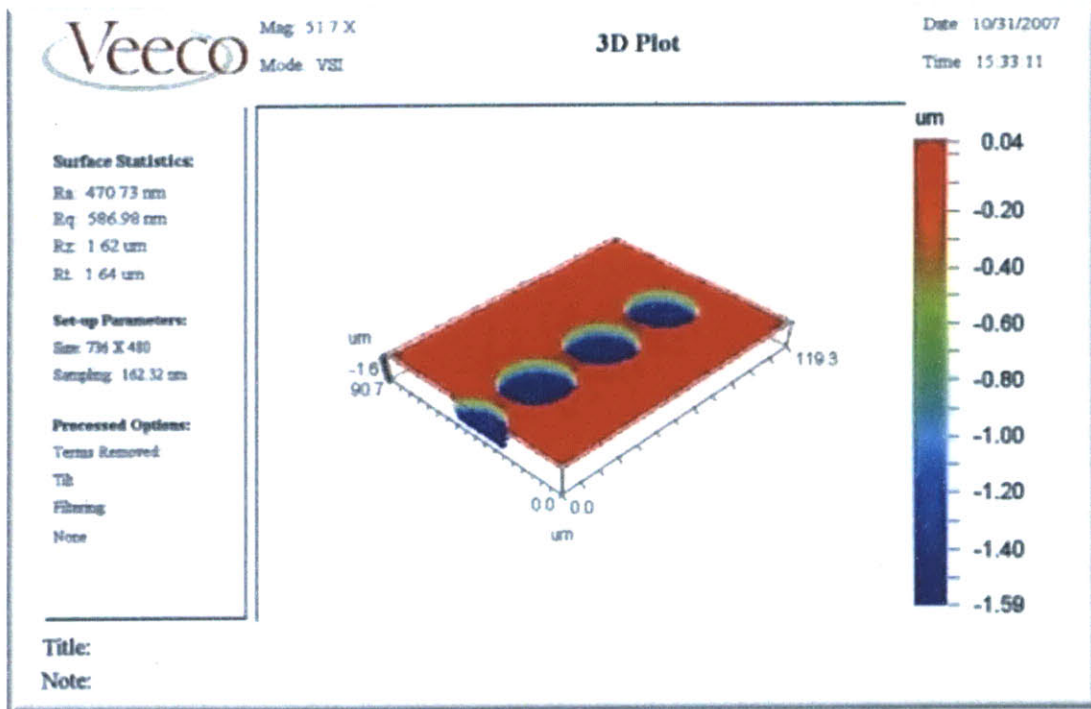


Figure 5.3 – 3-D image from optical interferometry of “circle” structures.

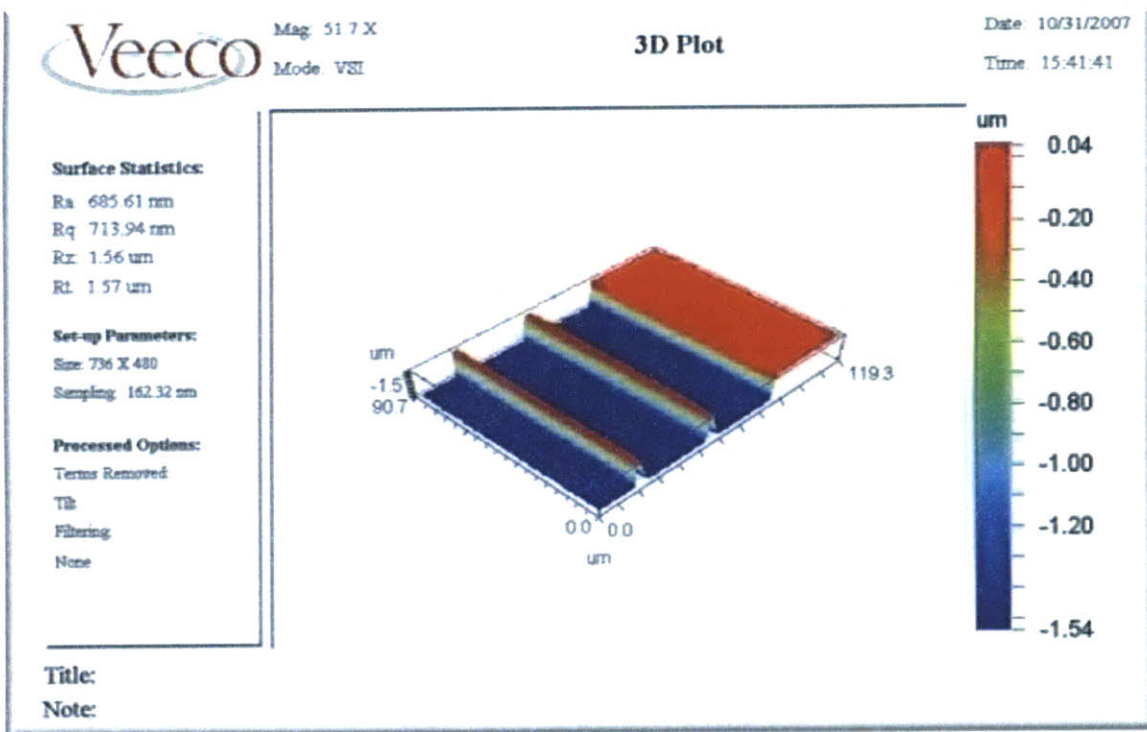


Figure 5.4 – 3-D image from optical interferometry of “channel” structures.

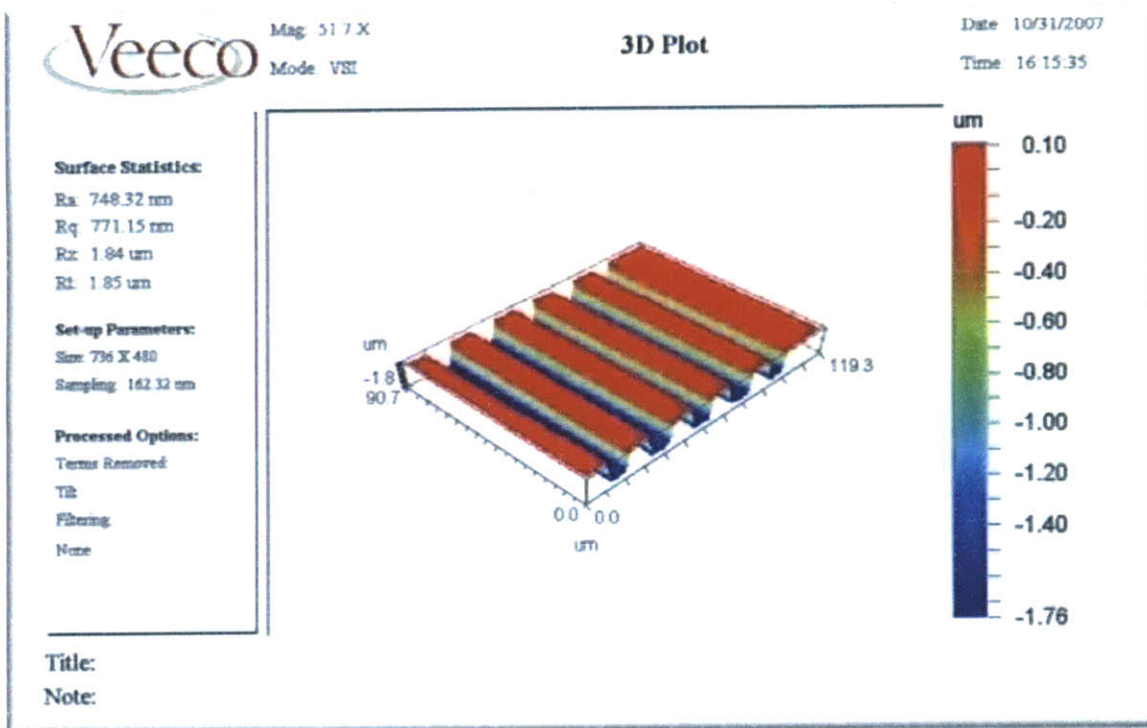


Figure 5.5 – 3-D image from optical interferometry of “channel” structures.

## 5.2 Scanning electron microscope

All the critical dimension measurements are taken using a scanning electron microscope. The electron microscope images the sample surface by scanning it with a high-energy beam of electrons in a raster scan pattern. The electrons interact with the atoms that make up the sample, producing signals that contain information about the sample's surface topography. A few of the images taken by SEM are shown in Figures 5.6 to 5.11.

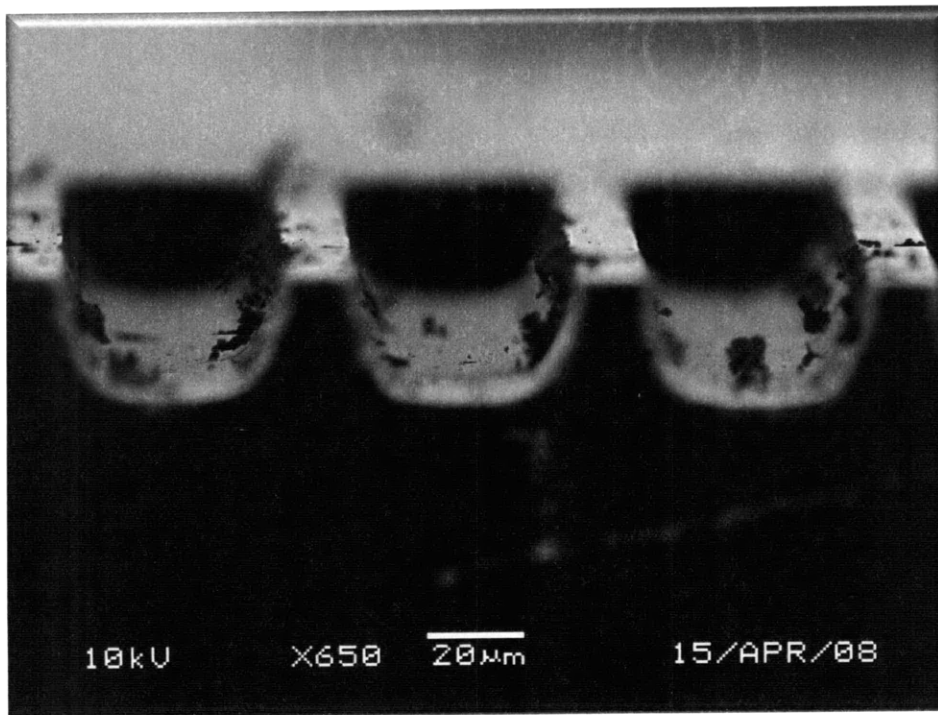
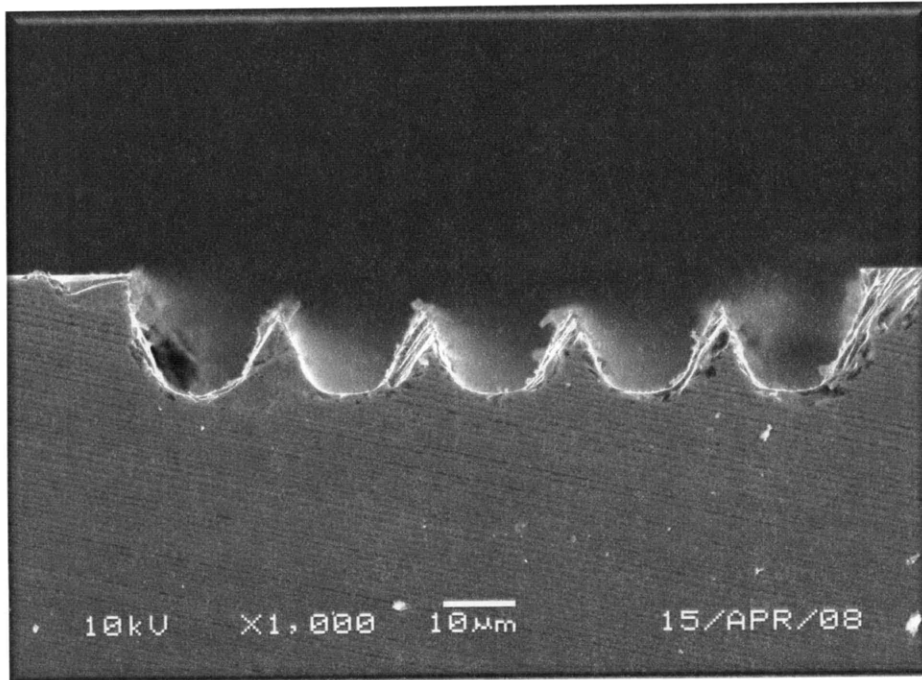
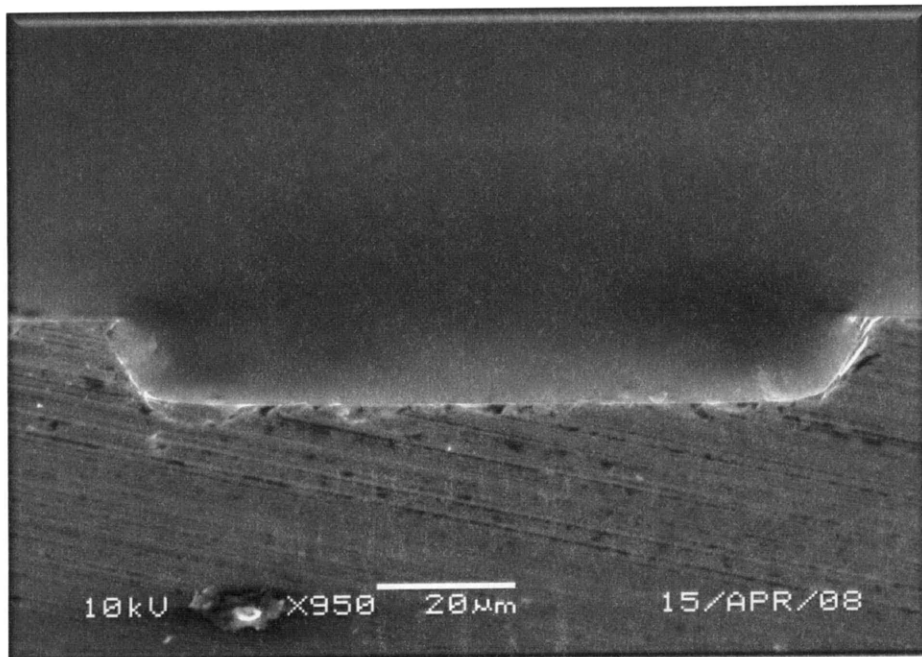


Figure 5.6 – An SEM image of the “channel” structures with line width= 30 µm.





**Figure 5.7 – An SEM image of “channel” structures with line width = 10  $\mu\text{m}$ ; the long etch time resulted in over-etching the sidewalls.**



**Figure 5.8 – An SEM image of a “channel” structure with line width = 100  $\mu\text{m}$ ; the small aspect ratio resulted in straight, non-vertical sidewalls.**

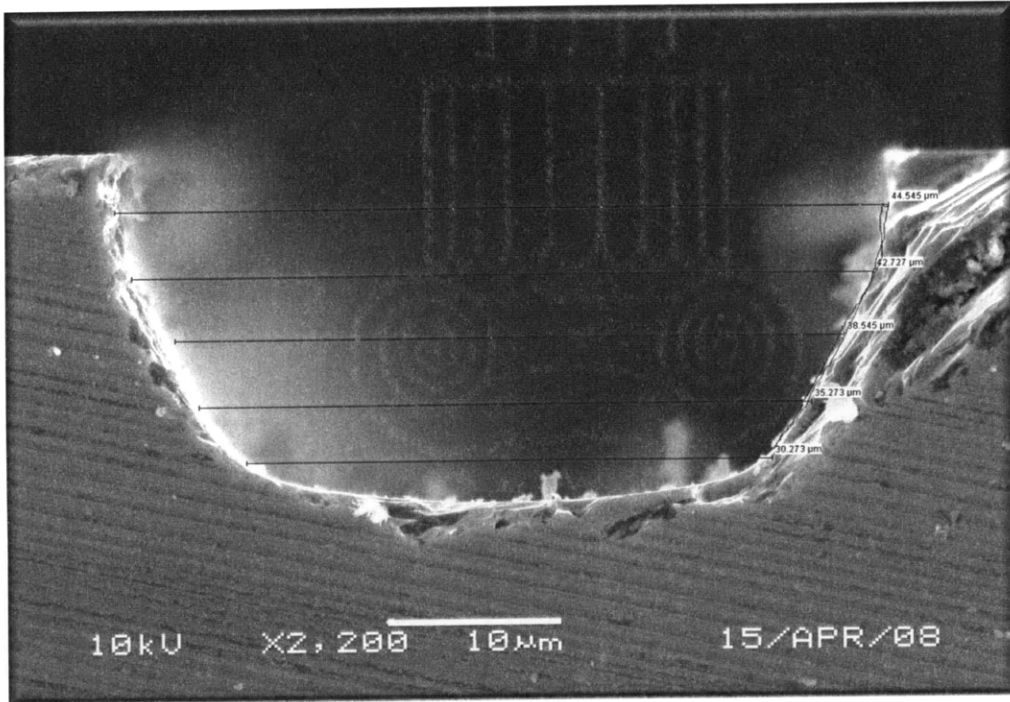


Figure 5.9 – An SEM image of a “channel” structure with line width = 30  $\mu\text{m}$ ; the large aspect ratio resulted in quadratic-shaped sidewalls. The blue lines show multiple width measurements on the sidewall.

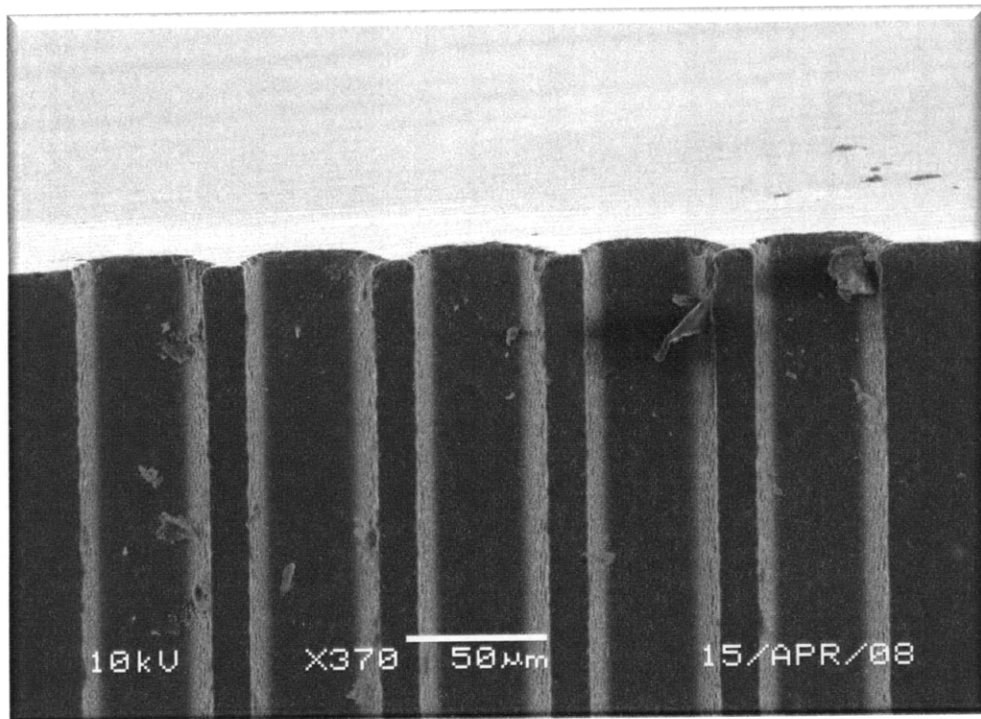
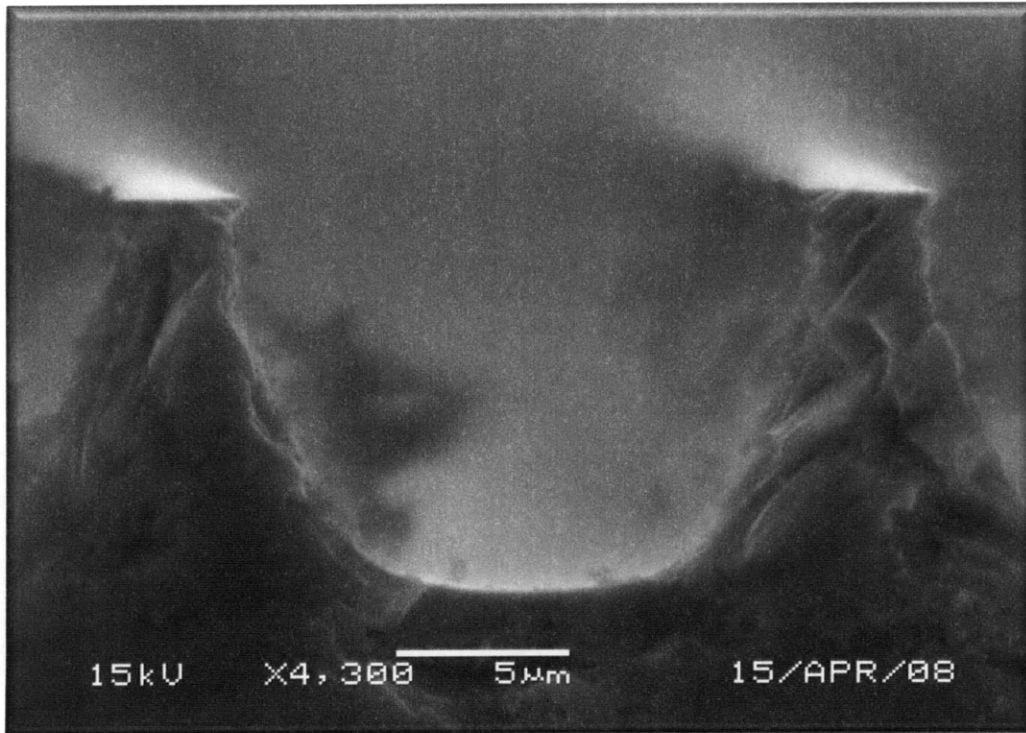


Figure 5.10 – A top-view SEM image of “channel” structures with line width = 30  $\mu\text{m}$ .



**Figure 5.11 – An SEM image of a “channel” structure with line width = 10 µm.**

The summary of data from optical interferometry and SEM measurements is presented in Appendix A.

## Chapter 6

### Etch Rate Model: Data and Fitting

This chapter applies the etch rate model developed in Chapter 3 to the data taken from the DRIE experiment. The goal of the chapter is evaluating the level of accuracy of the etch rate model and fitting the physical parameters in Equation 3-10 to match the measurements. In the first section, the optimized effective pattern density of the mask is calculated. In the second section, time evolution of etch rate is described using the experimental data, and in the third section lateral etch is used to extract the complete set of values for physical parameters.

#### 6.1 Pattern dependency of etch rate

The improved model for the etch rate from Chapter 3 has the form:

$$t = \left( \gamma \frac{z^2}{2R_0 \cdot CD} s_{bottom} + \frac{z}{R_0} \left( 1 + \frac{s_{side} \cdot s_{bottom}}{1 - s_{side}} \right) \right) e^{\alpha \rho_{eff}(x,y)^\beta} \quad (6-1)$$

Since it is computationally costly to optimize all six parameters at once, a faster approach is adopted. In this approach, first only  $\alpha$ ,  $\beta$  and  $c$  are optimized, together with  $R_0$ . To achieve this goal Equation 6-1 needs to be reduced to an equation that only includes these four parameters. Considering the derivation of Equation 6-1 in Chapter 3, we see that if features with very low aspect ratios are concerned then Equation 6-1 reduces to:

$$z = t \cdot R_0 e^{-\alpha \rho_{eff}^\beta} \quad (6-2)$$

Equation 6-2 is simply stating that for very small aspect ratios (i.e. in the beginning of the etch process) the etch rate is constant over that time and varies over the die based on pattern density dependency. By isolating the four desired parameters ( $c$  being implicit in  $\rho_{eff}$ ), Equation 6-2 enables us to simplify the MATLAB optimization.

Figure 6.1 shows the experimental data from the shallow etched wafer ( $t = 40$  sec) and the optimized simulation. The simulation reaches a root mean square (rms) error down to 2.8%. Table 6.1 shows the values for the optimized parameters.

$R_0 = 49.8 \text{ nm/sec}$ $\alpha = 0.19$ $\beta = 2.9$ $c = 186 \mu\text{m}$
--

**Table 6.1 – Fitting the model parameters to match the data gives numeric value for four of the parameters.**

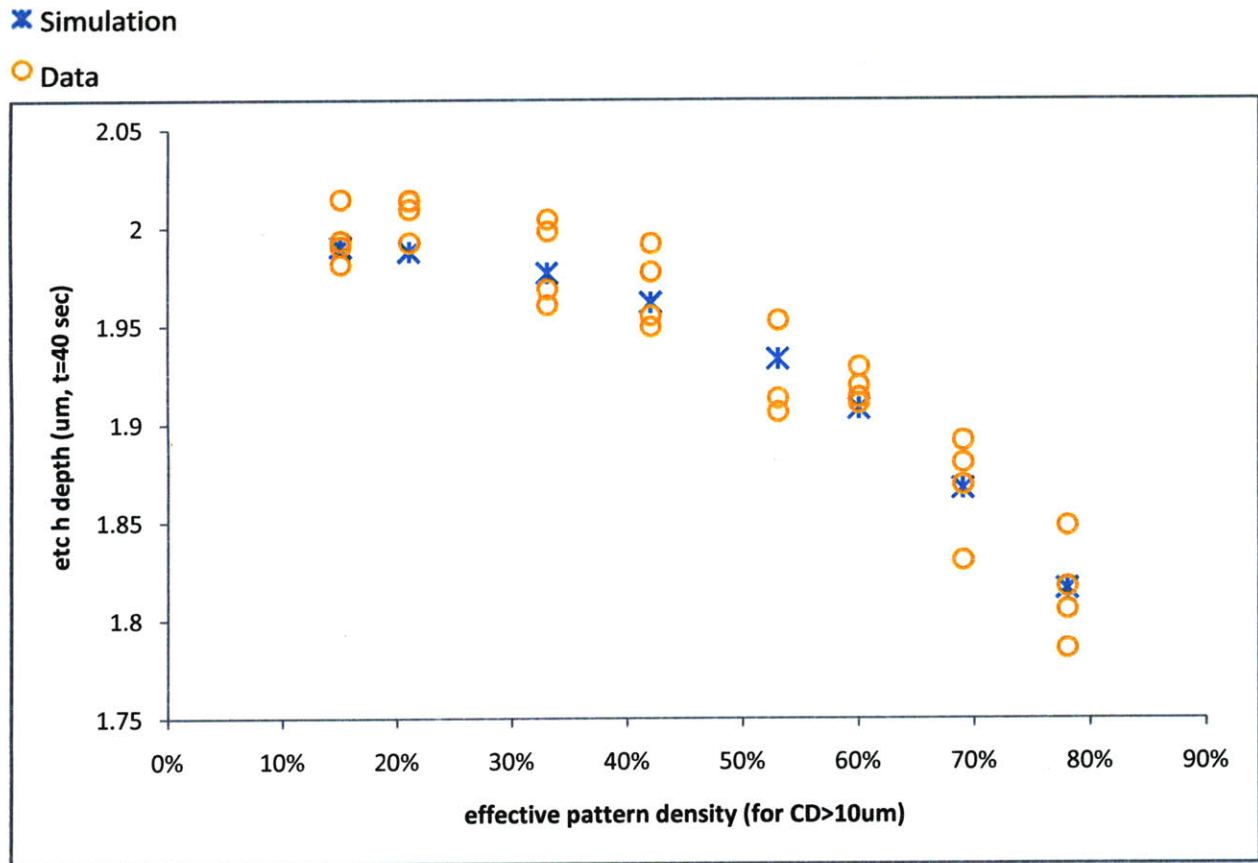


**Figure 6.1 – Etch depth data for wafer #1 and the optimized simulation.**

## 6.2 Time evolution of etch rate

The improved equation for the etch rate for longer etch times (where ARDE effects are also important) can be written in the short form:

$$t = A \frac{z^2}{CD} + Bz \quad (7-1)$$

where  $A$  and  $B$  will be optimized to match the experimental data. The physical parameters including the sticking factors to the side wall and the bottom, will be calculated from  $A$  and  $B$ . To take full advantage of the time dependent etch rate model, Equation 7-1 is applied to the time evolution of three distinct features. Figures 6.2 to 6.4 show this result; for 50% pattern density features with  $CD$  of  $3 \mu\text{m}$ ,  $30 \mu\text{m}$ , and  $10 \mu\text{m}$ .

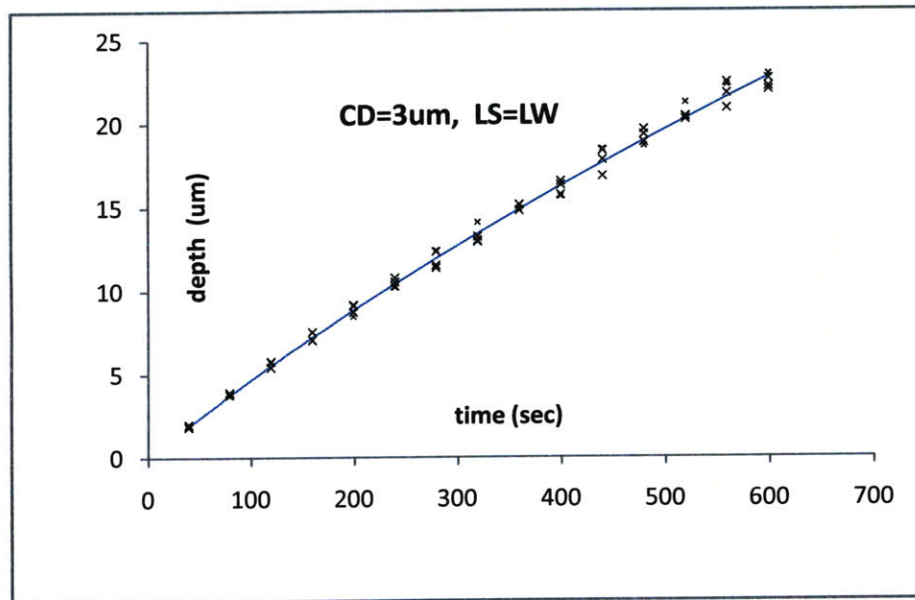


**Figure 6.2 – Etch depth for a “channel” feature with  $CD=3 \mu\text{m}$ , data (black x) are from four dies within each wafer and the blue line shows the optimized simulation.**

The depth of each feature is measured for four dies within 15 wafers to span the whole timeline from 40 seconds to 600 seconds of etching exposure time. The blue line in each graph shows the best simulation with a minimum rms error of 3.6 % overall.

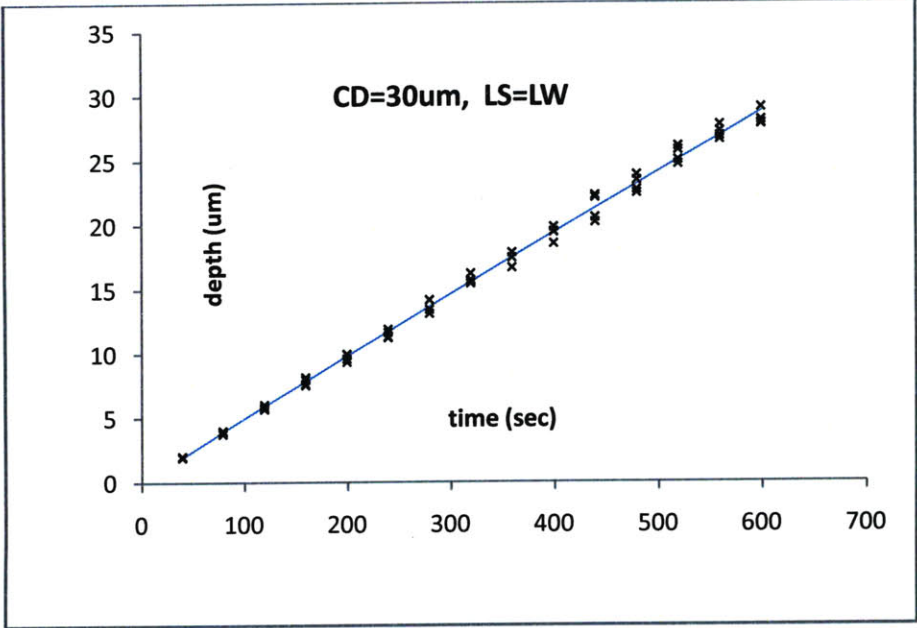


Figure 6.3 – Etch depth for a “channel” feature with CD= 30 μm, data (black x) are from four dies within each wafer and the blue line shows the optimized simulation.

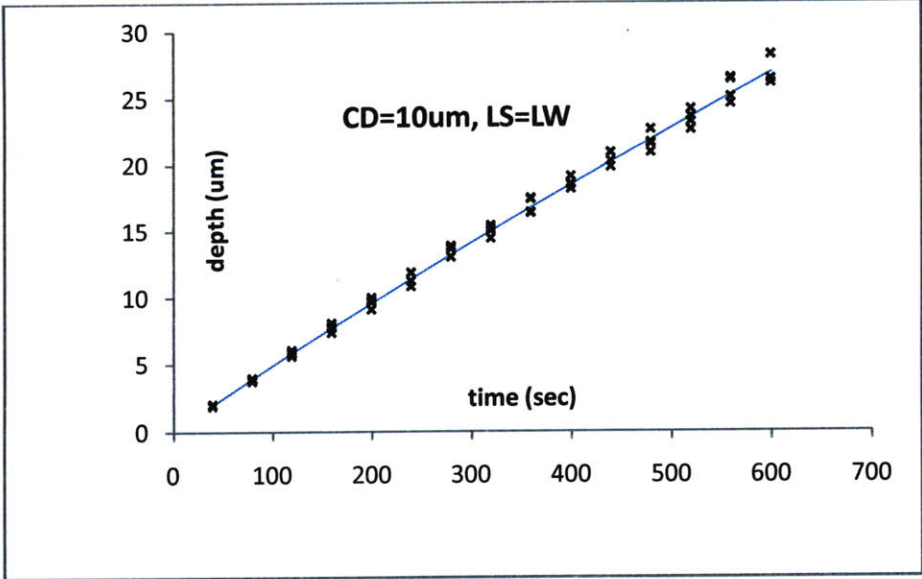
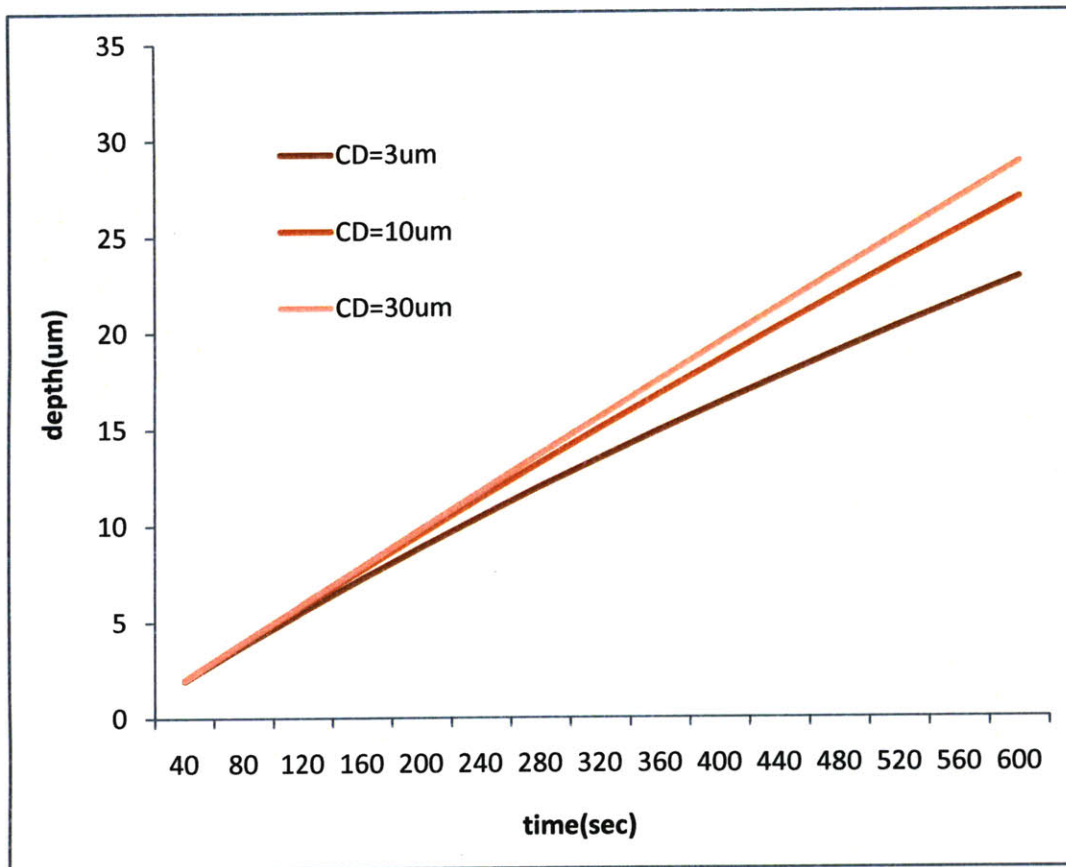


Figure 6.4 – Etch depth for a “channel” feature with CD= 10 μm, data (black x) are from four dies within each wafer and the blue line shows the optimized simulation.



Figure 6.5 shows the simulation results for all the three features together. As expected, the deviation of the etch depth from a linear equation is higher for features with higher aspect ratios. In particular, the narrowest CD of 3  $\mu\text{m}$  shows a substantial quadratic roll-off in depth versus time due to ARDE effects.



**Figure 6.5 – The optimized simulation of etch depth as a function of time for three different line width; the narrowest line width (3  $\mu\text{m}$ ) has the largest quadratic roll-off.**



### 6.3 Lateral etch rate

In Chapter 3 the lateral etch rate was formulated and introduced as a major improvement to the previous etch models. The following equations describe the lateral etch profile for shallow features (small aspect ratios)

$$x(z) \approx \frac{S_{side}}{S_{bottom}} R_0 (T_{total} - t(z)) \quad (8-1)$$

$$t(z) = \frac{z}{R_0} e^{\alpha \rho_{eff}^\beta} \quad (8-2)$$

Equations 8-1 and 8-2 suggest that the lateral etch rate is constant over time for the shallow features, and therefore the profile of this feature will have a linear shaped side wall. This prediction is confirmed in the images taken from the shallow features, as shown in Figure 6.6.



**Figure 6.6 – The sidewall profile for a feature with very small aspect ratio; the sidewall is straight.**

Equations 8-1 and 8-2 predict that the ratio of the sticking factors to the side wall and to the bottom is determined by the slope of the side wall edge (the orange line in Figure 6.6). The profile measurements are taken for the feature shown in Figure 8.1 from all of the four dies. The

results are shown in Figure 6.7. The blue line represents the best fit (with rms error of 6.1%) for the profile measurement. The slope of the blue line determines the ratio of the sticking factors to the side wall and to the bottom. In our data, this ratio is determined to be  $0.262 \pm 0.016$  (where 0.016 is the standard error in the fit to the data of Figure 6.7).

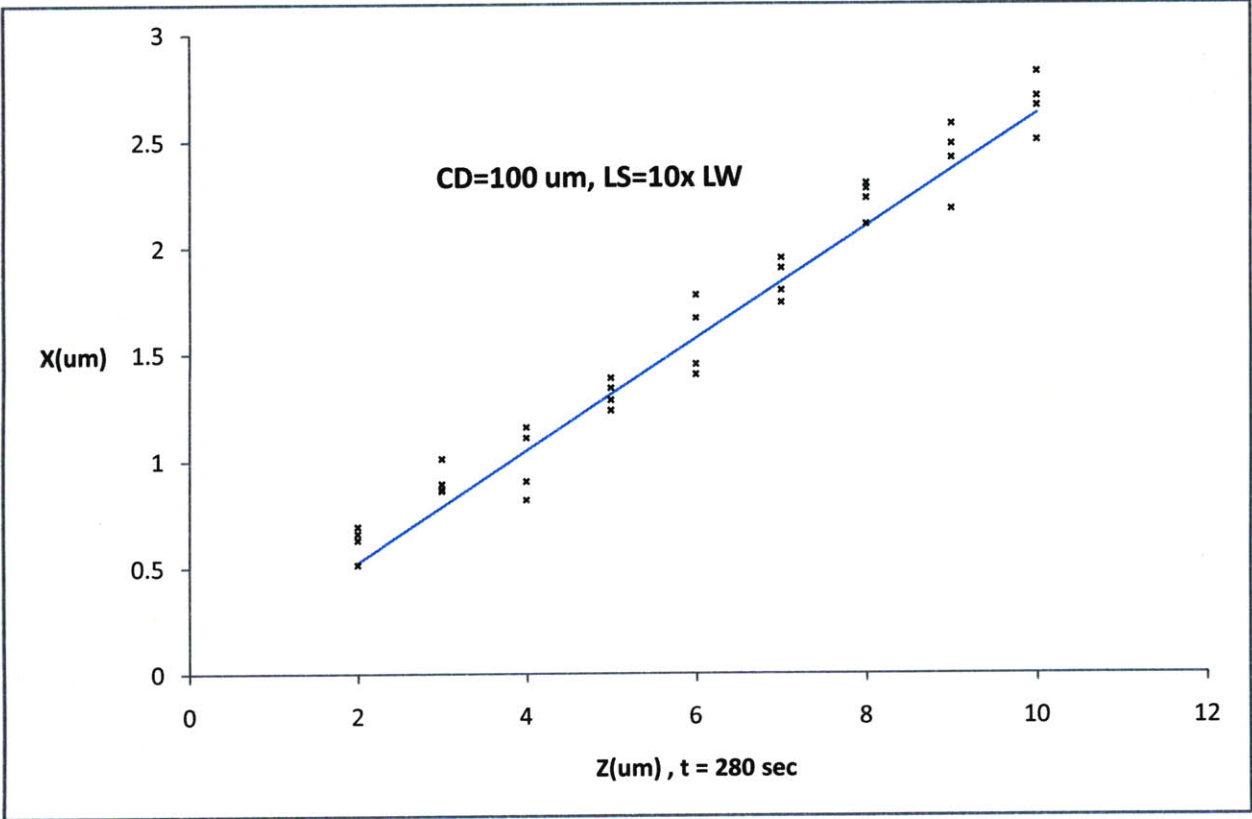


Figure 6.7 – The lateral etch  $x$  for the sidewall as a function of depth  $z$ , blue line shows the best linear fit.

## Chapter 7

### Integrated Model for Time Dependent Etching

The results from the partial fits in the previous two sections are combined with a full MATLAB optimization to match the experimental data to the remaining parameters, to extract values for  $s_{bottom}$ ,  $s_{side}$ , and  $\gamma$ . The following values for the physical parameters result:

$$\begin{aligned} R_0 &= 49.8 \text{ nm/sec} & s_{bottom} &= 0.141 \\ \alpha &= 0.19 & s_{side} &= 0.037 \\ \beta &= 2.9 & \gamma &= 0.58 \\ c &= 186 \mu\text{m} \end{aligned}$$

These parameters complete the improved model for the time dependent etch rate:

$$t = \left( \gamma \frac{z^2}{2R_0 \cdot CD} s_{bottom} + \frac{z}{R_0} \left( 1 + \frac{s_{side} \cdot s_{bottom}}{1 - s_{side}} \right) \right) e^{\alpha \rho_{eff}(x,y)^\beta} \quad (7-1)$$

Based on this model, the etch rate varies with both pattern density and aspect ratio. Also the time evolution of the etch depth is characterized by the quadratic equation that is based on the physics behind the sticking factors. The sticking factor for the bottom is higher than the sticking factor for the side wall; as expected the side wall etch is a perturbation to the vertical etch model. Intuitively the lateral etch is substantially slower than the vertical etch due to the fact that the flux of the neutral reactants is not unidirectional; it is essentially directed downward. In addition, these coefficients may also encompass some effects of ion directionality. Equation 7-1 can also be solved simple to give the etch depth as a function of time giving:

$$z = \frac{CD}{2} \left( \sqrt{2\gamma \frac{s_{bottom}}{CD} R_0 \cdot t \cdot e^{-\alpha \rho_{eff}(x,y)^\beta} + \left( 1 + \frac{s_{side} \cdot s_{bottom}}{1 - s_{side}} \right)^2} - \left( 1 + \frac{s_{side} \cdot s_{bottom}}{1 - s_{side}} \right) \right) \quad (7-2)$$

## Chapter 8

### Conclusions and Future Work

Pattern density dependency and aspect ratio dependent etching are two main causes for non-uniformities in plasma etching. This thesis contributes a physical analysis to describe an integrated model for these two effects that also considers the time evolution of the etch rate and the effect of lateral etch on non-uniformities.

The experimental data from the Deep Reactive Ion Etching experiments were described through the eyes of the improved integrated model for etch rate. Further improvements may include exploring the wafer-level variations in the etch rate, and conducting lateral etch-only processes to identify the characteristics for the lateral etch rate and its effect on the overall uniformity.

Wafer-level non-uniformities could dominate the local variations in etch rate. The global map of etch rate is dependent on various wafer-level parameters such as pressure, ICP asymmetries and also average pattern density of the wafer. Understanding these effects is crucial for developing a complete picture for plasma etching non-uniformities.

This thesis emphasizes the negative effect of lateral etch on vertical etch uniformity. It is fruitful to implement a time-based model for lateral etch rate. Wafers with etch-stop layers can be used to decouple time evolution of lateral etch from that of vertical etch. It is worthwhile to notice that lateral etch could alter not only ARDE effect but also pattern density (micro-loading) effect by increasing the overall etch surface.

## Appendix A

etch time (sec)	etch depth ( $\mu\text{m}$ )											
	CD = 3 $\mu\text{m}$				CD = 10 $\mu\text{m}$				CD = 30 $\mu\text{m}$			
	die1	die 2	die3	die4	die1	die 2	die3	die4	die1	die 2	die3	die4
40	1.85	1.90	2.01	2.03	1.93	2.06	2.04	2.01	2.07	1.98	1.99	1.98
80	3.94	3.81	3.92	3.76	3.77	3.97	3.95	3.90	4.04	3.93	3.80	3.97
120	5.77	5.80	5.45	5.75	6.09	5.62	5.80	5.92	5.73	5.86	5.73	6.05
160	7.07	7.07	7.60	7.57	7.90	8.11	7.74	7.39	8.20	7.99	7.68	7.57
200	8.76	9.20	9.13	8.51	9.83	9.13	10.02	9.70	9.98	10.00	9.39	9.63
240	10.80	10.57	10.32	10.24	11.27	11.90	11.89	10.85	11.34	11.28	11.70	11.95
280	11.40	11.56	12.37	12.44	13.88	13.04	13.67	13.85	13.48	14.21	14.24	13.17
320	13.03	13.26	12.96	14.12	15.05	14.44	15.44	15.23	15.78	16.27	15.66	15.49
360	15.16	14.80	15.14	14.93	17.49	16.44	17.41	16.36	17.49	16.72	17.90	17.89
400	16.34	15.75	16.55	15.66	19.13	18.18	18.56	18.52	18.58	19.52	19.47	19.87
440	16.86	18.37	17.82	18.46	19.82	20.93	20.29	20.95	20.60	20.24	22.16	22.33
480	19.36	18.87	19.64	18.66	21.73	22.70	20.94	21.61	22.76	22.49	23.93	23.51
520	20.39	20.43	20.23	21.25	22.68	23.65	23.26	24.19	24.73	25.83	26.16	25.07
560	20.91	21.80	22.47	22.32	26.52	25.07	26.39	24.57	27.78	26.90	27.30	26.62
600	22.21	22.68	22.02	22.95	28.23	28.25	26.13	26.41	28.12	29.08	27.88	27.80

**Table A.1 – Summary of the optical interferometry measurements.**

depth ( $\mu\text{m}$ )	lateral etch ( $\mu\text{m}$ ), CD = 100 $\mu\text{m}$			
	die1	die2	die3	die4
2.0	0.66	0.63	0.70	0.52
3.0	1.01	0.87	0.86	0.89
4.0	1.11	0.91	0.82	1.16
5.0	1.39	1.24	1.29	1.34
6.0	1.67	1.78	1.45	1.40
7.0	1.80	1.95	1.74	1.90
8.0	2.30	2.23	2.11	2.28
9.0	2.58	2.18	2.42	2.49
10.0	2.82	2.66	2.50	2.71

**Table A.2 – Summary of the SEM measurements.**

## References

- [1] K. Abrokwah, "Plasma-etch pattern dependencies in integrated circuits," MIT Master of Engineering thesis, Feb. 2006.
- [2] H. Sun, T. Hill, M. Schmidt, and D. Boning, "Characterization and Modeling of Wafer and Die Level Uniformity in Deep Reactive Ion Etching (DRIE)," *2003 MRS Fall Meeting*, Boston, MA, Dec. 2003.
- [3] P. Clausing, "The Flow of Highly Rarefied Gases through Tubes of Arbitrary Length," *J. Vac. Sci. Technology*, vol. 8, no. 5, pp. 636-646, 1931.
- [4] R. A. Gottscho and C. W. Jurgensen, "Microscopic Uniformity in Plasma Etching," *J. Vac. Sci. Technology B*, vol. 10, no. 5, pp. 2133-2147, Sept./Oct. 1992.
- [5] T. Hill, H. Sun, H. Taylor, M. Schmidt, and D. Boning, "Pattern Density Based Prediction for Deep Reactive Ion Etch (DRIE)," *Tech. Digest of 2004 Hilton Head Solid-State Sensors and Actuators Workshop*, Hilton Head Island, SC, 2004.
- [6] J. W. Coburn and H. F. Winters, "Conductance considerations in the reactive ion etching of high aspect ratio features," *Appl. Phys. Lett.*, vol. 55, no. 26, pp. 2730-2732, Dec. 1989.
- [7] I. W. Rangelow, "Critical tasks in high aspect ratio silicon dry etching for microelectromechanical systems," *J. Vac. Sci. Technol., A*, vol.21, no.4, pp. 1550-1562, 2003.
- [8] W. N. G. Hitchon, Plasma Processes for Semiconductor Fabrication, Cambridge: Cambridge University Press, pp. 62-65, 1999.
- [9] J. Lee, W. Lim, I. Baek, and G. Cho, "Advance high density plasma processing in inductively coupled plasma systems for plasma-enhanced chemical vapor deposition and dry etching of electronic materials," *J. Ceramic Processing Research.*, vol. 4, no. 4, pp. 185-190, 2003.
- [10] N. Fujiwara, H. Sawai, M. Yoneda, K. Nishioka, and H. Abe, "ECR Plasma Etching with Heavy Halogen Ions," *Jpn. J. Appl. Phys.*, vol. 29, part 1, no. 10, pp. 2223-2228, 1990.